Molecular Therapy
Methods & Clinical Development
Original Article

Persistent tailoring of MSC activation through genetic priming

Michael A. Beauregard,[1] Guy C. Bedford,[1] Daniel A. Brenner,[1] Leonardo D. Sanchez Solis,[1] Tomoki Nishiguchi,[3] Abhimanyu,[3] Santiago Carrero Longlax,[3] Barun Mahata,[1] Omid Veiseh,[1] Pamela L. Wenzel,[5,6,7] Andrew R. DiNardo,[3,4] Isaac B. Hilton,[1] and Michael R. Diehl[1,2]

[1]Department of Bioengineering, Rice University, Houston, TX, USA; [2]Department of Chemistry, Rice University, Houston, TX, USA; [3]The Global Tuberculosis Program, Texas Children's Hospital, Immigrant and Global Health, WTS Center for Human Immunobiology, Department of Pediatrics, Baylor College of Medicine, Houston, TX, USA; [4]Department of Internal Medicine and Radboud Center for Infectious Diseases, Radboud University Medical Center, Nijmegen, the Netherlands; [5]Department of Integrative Biology & Pharmacology, The University of Texas Health Science Center at Houston, Houston, TX, USA; [6]Center for Stem Cell and Regenerative Medicine, Brown Foundation Institute of Molecular Medicine, The University of Texas Health Science Center at Houston, Houston, TX, USA; [7]Immunology Program, The University of Texas MD Anderson UTHealth Graduate School of Biomedical Sciences, Houston, TX, USA

Mesenchymal stem/stromal cells (MSCs) are an attractive platform for cell therapy due to their safety profile and unique ability to secrete broad arrays of immunomodulatory and regenerative molecules. Yet, MSCs are well known to require preconditioning or priming to boost their therapeutic efficacy. Current priming methods offer limited control over MSC activation, yield transient effects, and often induce the expression of pro-inflammatory effectors that can potentiate immunogenicity. Here, we describe a genetic priming method that can both selectively and sustainably boost MSC potency via the controlled expression of the inflammatory-stimulus-responsive transcription factor interferon response factor 1 (IRF1). MSCs engineered to hyper-express IRF1 recapitulate many core responses that are accessed by biochemical priming using the proinflammatory cytokine interferon-γ (IFN-γ). This includes the upregulation of anti-inflammatory effector molecules and the potentiation of MSC capacities to suppress T cell activation. However, we show that IRF1-mediated genetic priming is much more persistent than biochemical priming and can circumvent IFN-γ-dependent expression of immunogenic MHC class II molecules. Together, the ability to sustainably activate and selectively tailor MSC priming responses creates the possibility of programming MSC activation more comprehensively for therapeutic applications.

INTRODUCTION

Mesenchymal stem/stromal cells (MSCs) are widely recognized for their potential for treating diverse classes of human diseases and disorders.[1] The efficacy of MSCs or their cell-free products[2,3] has been studied in hundreds of clinical trials[4] across multiple settings spanning neurodegenerative disorders,[5] inflammatory bowel disease,[6] cardiac diseases,[7] coronavirus disease 2019,[8] and others. This broad potential stems from the ability of MSCs to simultaneously express and secrete a spectrum of different pleiotropic immunomodulatory and regenerative chemokines, cytokines, growth factors, metabolites, and vesicles.[9,10] Virtually all MSC-based cell therapies seek to leverage the delivery of these effector molecules to suppress inflammation, restore immune homeostasis, and promote healing.[11,12]

Despite their promise, MSC therapies have shown limited clinical efficacy.[13] Multiple factors contribute to this deficiency, many of which can be linked to insufficient cell potency.[4,14] Overall, it is widely accepted that MSCs must be primed biochemically[15,16] or biophysically[17,18] to activate and/or enhance their production of immune effector molecules since basal unstimulated MSCs do not typically produce these molecules in sufficient quantities. Pro-inflammatory stimuli including cytokines such as interferon γ (IFN-γ), tumor necrosis factor α (TNF-α), and interleukin 1β (IL-1β) or pathogenic molecules such as lipopolysaccharide,[19] individually and in combination,[20] have been explored extensively due to their ability to mimic natural priming of MSCs by activated immune cells during infections or injuries.[21] These molecules induce comprehensive changes to the MSC transcriptome, proteome, and secretome[22] via the activation of stimulus-responsive transcription factors (TFs).[15] As a key example, IFN-γ bolsters MSC potency through the TF signal transducer of activation 1 (STAT1).[23] Stimulation with IFN-γ activates STAT1 phosphorylation, dimerization, and translocation to the nucleus, where it binds to gamma-activated sequences within the promoters of many different IFN-stimulated genes (ISGs).[24–26] This includes additional TFs that can function as signaling intermediates, like IFN response factor 1 (IRF1), which further broaden transcriptional responses to IFN-γ signaling by binding to IFN-stimulated response elements within the promoters of additional IRGs, notably with and/or without STAT1.[27,28] Among other effectors, IRF1 is well known to regulate indoleamine 2,3-dioxygenase 1 (IDO1),[29,30]

Received 28 March 2024; accepted 5 August 2024;
https://doi.org/10.1016/j.omtm.2024.101316.

Correspondence: Michael R. Diehl, Department of Bioengineering, Rice University, Houston, TX, USA.
E-mail: diehl@rice.edu

which is recognized as a key determinant of the immunosuppressive potency of MSCs.[31–33]

Although biochemical and biophysical/biomechanical priming methods have both been shown to boost MSC bioactivity and improve therapeutic responses, several challenges remain that affect the functionality and durability of primed MSCs. In particular, MSC activation tends to be transient and short lived.[34] The effect of biochemical priming by IFN-γ and other stimulants has been shown to decay within a few days in stimulus washout experiments.[35] More persistent activation has been achieved using engineered biomaterials that integrate the slow release of IFN-γ to provide constant stimulation.[34] Yet, biochemical stimulation is also difficult to modify and can induce the expression of unwanted and deleterious immunogenic and/or proinflammatory effectors.[36,37] For example, in addition to other proinflammatory factors, IFN-γ strongly induces the expression of the transcriptional coactivator class II transcriptional activator (CIITA).[38] CIITA, in turn, upregulates the expression of multiple major histocompatibility complex (MHC) class II molecules that can potentiate MSC immunogenicity and promote MSC clearance by CD4 T cells.[39]

MSCs have been genetically engineered to constitutively overexpress transgenes encoding for different effector molecules including IDO1,[40] COX-2,[41] and other effectors.[42] While constitutive overexpression of these molecules can address the durability of MSC activation, current genetic engineering technologies can typically only manipulate the expression of a few genes at a time, far less than the number of genes that are activated via biochemical or biomechanical stimuli. The multifaceted secretome of MSCs, especially of primed MSCs, facilitates regulation of multiple classes of immune and immune-supporting cells,[43] and this is among the unique properties that make MSCs attractive candidates for cell therapy.

Here, we demonstrate that stable hyperexpression of IRF1 can be leveraged to upregulate broad arrays of immunomodulatory effector genes and recapitulate the potency gains that can be achieved via traditional biochemical priming with IFN-γ. However, genetic priming via IRF1 was also shown to circumvent the activation of STAT1 and key STAT1-dependent downstream ISGs like CIITA. In contrast with IFN-γ-primed cells, this effect was associated with low MHC class II gene expression and improved retention of MSC hypo-immunogenicity in MSC-peripheral blood mononuclear cell (PBMC) coculture assays. Finally, sustained (>21-day) priming was also demonstrated in primary human adipose-derived MSCs (AD-MSCs), where activated IDO1 production was maintained for weeks. Together, these results demonstrate that the engineered expression of intermediate TFs like IRF1 can facilitate selective and persistent programming of MSCs in ways that activate large numbers of therapeutically relevant effector molecules while minimizing the activation of other molecules that have the potential to impair therapeutic efficacy. Such control may open routes to better tailor and maintain the activated phenotypes of MSCs for specific therapeutic applications.

RESULTS

IRF1 overexpression mimics key activation signatures of IFN-γ priming

The usefulness of IRF1 transgenes for priming was first tested using immortalized hTERT-MSCs that were transduced (multiplicity of infection [MOI] = 1) with a lentiviral vector that encoded for a full length IRF1 transgene and eGFP (Figures 1A, 1B, and S1). The resulting IRF1-overexpressing cells (MSC^{IRF1}) displayed enhanced IRF1 transcription, translation, and nuclear localization by RT-qPCR and immunocytochemistry (Figures 1C and 1D). Although biochemical stimulation with IFN-γ for 24 h ($MSC^{IFN\text{-}\gamma}$) induced higher transcription of endogenous IRF1 compared with MSC^{IRF1}, both methods yielded a more than 25,000-fold induction of IDO1 transcription (Figure 1D), which is a key ISG target of IRF1 and a signature of IFN-γ priming. IDO1 exerts immunomodulatory effects by converting tryptophan into kynurenine within the tryptophan metabolic pathway.[44] Kynurenine levels were also elevated using both priming techniques and were indistinguishable between MSC^{IRF1} and $MSC^{IFN\text{-}\gamma}$ ($p = 0.63$) (Figure 1E). Together these results demonstrate that IRF1 transgene expression in MSCs can recapitulate key activation signatures of IFN-γ stimulation.

IRF1 activates MSC-mediated T cell suppression

We next characterized and compared IRF1 and IFN-γ-induced changes to the MSC transcriptome using bulk RNA sequencing (RNA-seq) (Figures 2A–2D). Both priming methods induced transcriptional changes, yielding more than 1900 differentially expressed genes (DEGs), each relative to untreated control MSCs ($p < 0.05$) (fold change [FC] > 2) (Figures 2A–2C). In addition to *IDO1*, upregulated DEGs included *COX-2* (*PTGS2*), a second key immunomodulatory effector enzyme that produces the anti-inflammatory small molecule prostaglandin E2,[45] along with multiple effector genes associated with T cell suppression including *IL4I1*,[46] *Galactin-9*[47,48] (*LGALS9*), PD-L2[49] (*PDCD1LG2*), and *FGL2*[50] (Figure 2A). Along these lines, normalized enrichment scores from gene ontology (GO) analysis show transcription in both MSC^{IRF1} and $MSC^{IFN\text{-}\gamma}$ is positively enriched for genes corresponding with the GO terms "negative regulation of T cell proliferation" (0042130) and "negative regulation of T cell activation" (005086800) (Figures 2D and S2).

Consistent with their transcriptional profiles, IRF1- and IFN-γ-mediated priming were both demonstrated to enhance the immunosuppressive bioactivities of MSCs compared with basal, unprimed cells (Figures 2E–2G and S3). MSC conditioned media (CM) prepared using MSC^{IRF1} and $MSC^{IFN\text{-}\gamma}$ were shown to suppress the proliferation of PBMCs that were pre-stimulated with anti-CD3 and anti-CD28 antibodies to selectively activate T cells (Figures 2E and 2F). Finally, CM from $MSCs^{IRF1}$ was also found to decrease the percentage of CD4 T cells that positively expressed the activation marker TNF-α relative to CM from basal, unprimed MSCs (Figure 2G). As with the cell proliferation analyses, similar suppression of CD4 T cells was observed with MSC^{IRF1} and $MSC^{IFN\text{-}\gamma}$.

IRF1 hyperexpression maintains the immune evasive status of MSCs by circumventing STAT1 activation

RNA-seq also revealed marked differences between genetic and biochemical priming in the MSC^{IRF1} and $MSC^{IFN\text{-}\gamma}$ cells (Figures 2B–2D and 3A). In particular, genes from the GO term "T cell activation" (0042110) were depleted with MSC^{IRF1}, but positively enriched with $MSC^{IFN\text{-}\gamma}$ (Figure 2D). One of the most upregulated $MSC^{IFN\text{-}\gamma}$ genes in this GO term was CD74, or human leukocyte antigen (HLA) class II histocompatibility antigen γ chain CD74, involved in the assembly and trafficking of MHC class II complexes.[51] The expression of the transcriptional regulator *CIITA*, which again drives the downstream expression of MHC class II genes, was also significantly upregulated in $MSC^{IFN\text{-}\gamma}$ (FC = 126 ± 27) (p = 0.0002) but was much less so in MSC^{IRF1} (FC = 6 ± 1.4) (p = 0.008) (Figure 3A). In turn, while nearly all MHC class II genes were upregulated by IFN-γ treatment, HLA gene expression was largely unchanged by IRF1 overexpression (Figure 3A). Consistent with this behavior, flow cytometry analyses of the MHC class II cell surface receptor HLA-DR confirmed this result (Figures 3B and 3C). Here, while the level of HLA-DR was elevated slightly, compared with naive, unmodified MSCs, the geometric mean of HLA-DR expression in $MSC^{IFN\text{-}\gamma}$ was more than 35× that of MSC^{IRF1}.

To test if the above MHC class II expression changes would result in changes in immune reactivity, MSCs, $MSCs^{IFN\text{-}\gamma}$, and $MSCs^{IRF1}$ were next co-cultured in direct contact with unstimulated PBMCs. After 7 days, $CD4^+$ T cells showed an increase in activation status with $MSC^{IFN\text{-}\gamma}$ compared with MSC or MSC^{IRF1} (Figure 3D). There were 60% more TNF-α^+ CD4 T cells with $MSC^{IFN\text{-}\gamma}$ compared with MSC^{IRF1} and 70% more with $MSC^{IFN\text{-}\gamma}$ compared with untreated MSC. The PBMCs also proliferated 5.5× more with $MSC^{IFN\text{-}\gamma}$ compared with MSC^{IRF1} and 2.4× more with $MSC^{IFN\text{-}\gamma}$ compared with untreated MSC (Figure 3E).

IRF1 priming circumvents STAT1 activation

To gain mechanistic insight into the differences between genetic and biochemical priming, we next examined levels of STAT1 transcription, phosphorylation, and nuclear translocation in naive MSCs, MSC^{IRF1}, and $MSC^{IFN\text{-}\gamma}$ (Figure 4). IFN-γ was found to induce a much larger change in *STAT1* transcription (FC = 11 ± 0.35) (p = 0.0005) compared with IRF1 overexpression (FC = 3.0 ± 0.39) (p = 0.02) (Figure 4A). IFN-γ was also found to induce significant STAT1 phosphorylation by western blot (Figures 4B and S4) as expected.[15] In contrast, IRF1 overexpression resulted in much less STAT1 phosphorylation in MSCs that were cultured for at least 8 days after transduction. STAT1 activation is notably observed on day 4 in western blotting experiments (Figures S5A, S5C, and S5D), which we attribute to stimulation by the lentivirus. However, this signal dissipates by day 8 (Figures 4B and S5B), indicating that IRF1 overexpression does not sustain STAT1 activation on its own. IFN-γ also induced much more prominent pSTAT1 nuclear localization in immunocytochemical imaging experiments (Figures 4C and 4D). Together, these results suggest that the IRGs that are differentially expressed in MSC^{IRF1} cells relative to naive MSCs are indeed predominantly activated by IRF1 expression and not STAT1. They further suggest that differences between MSC^{IRF1} and $MSC^{IFN\text{-}\gamma}$ transcriptional profiles stem from the ability of IRF1 overexpression to

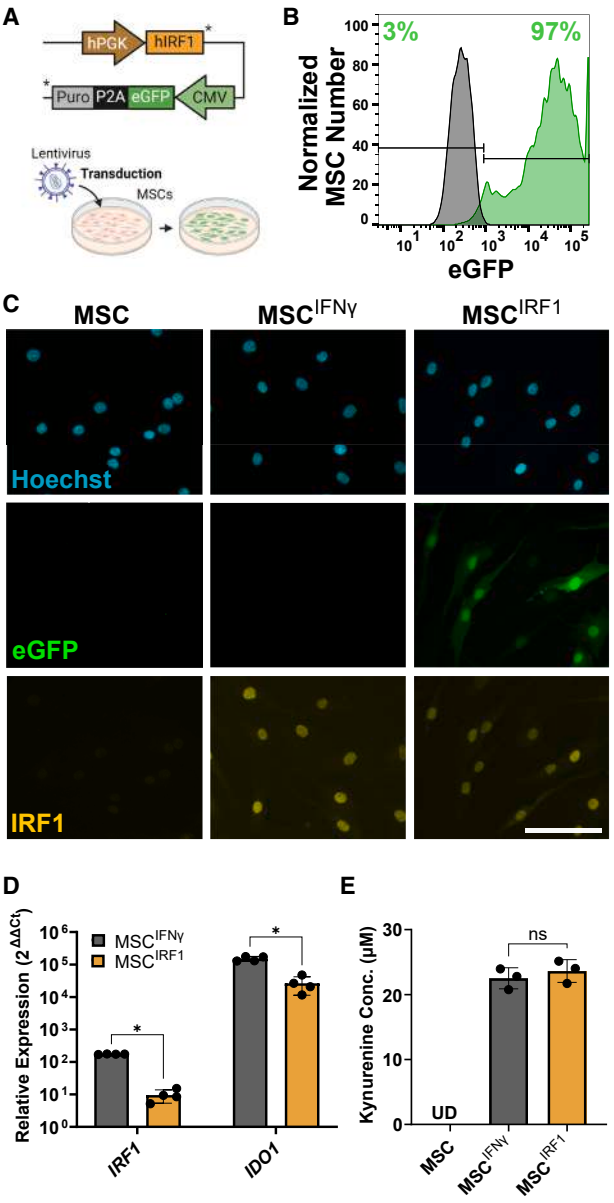

Figure 1. Genetic priming MSCS via overexpression of IRF1

(A) IRF1 lentiviral construct design. (B) Flow-based quantification of lentiviral transduction efficiency. Images were created using BioRender. (C) IRF1 transgene expression and IFN-γ stimulation at 50 ng/mL for 24 h both yield nuclear localization of IRF1. IRF1 was visualized by immunocytochemical staining. Scale bar, 100 μm. (D and E) IRF1 overexpression and IFN-γ stimulation (50 ng/mL for 24 h) both drive IDO1 transcription (D) and upregulate kynurenine production (E). Relative expression, $2^{\Delta\Delta Ct}$, in RT-qPCR analyses was calculated relative to unprimed MSCs for both $MSC^{IFN\text{-}\gamma}$ and MSC^{IRF1}. Statistical analyses were performed using multiple unpaired t tests. Kynurenine production was assayed using an Ehrlich reaction and analyzed using one-way ANOVA. *$p < 0.05$. Error bars represent the SD.

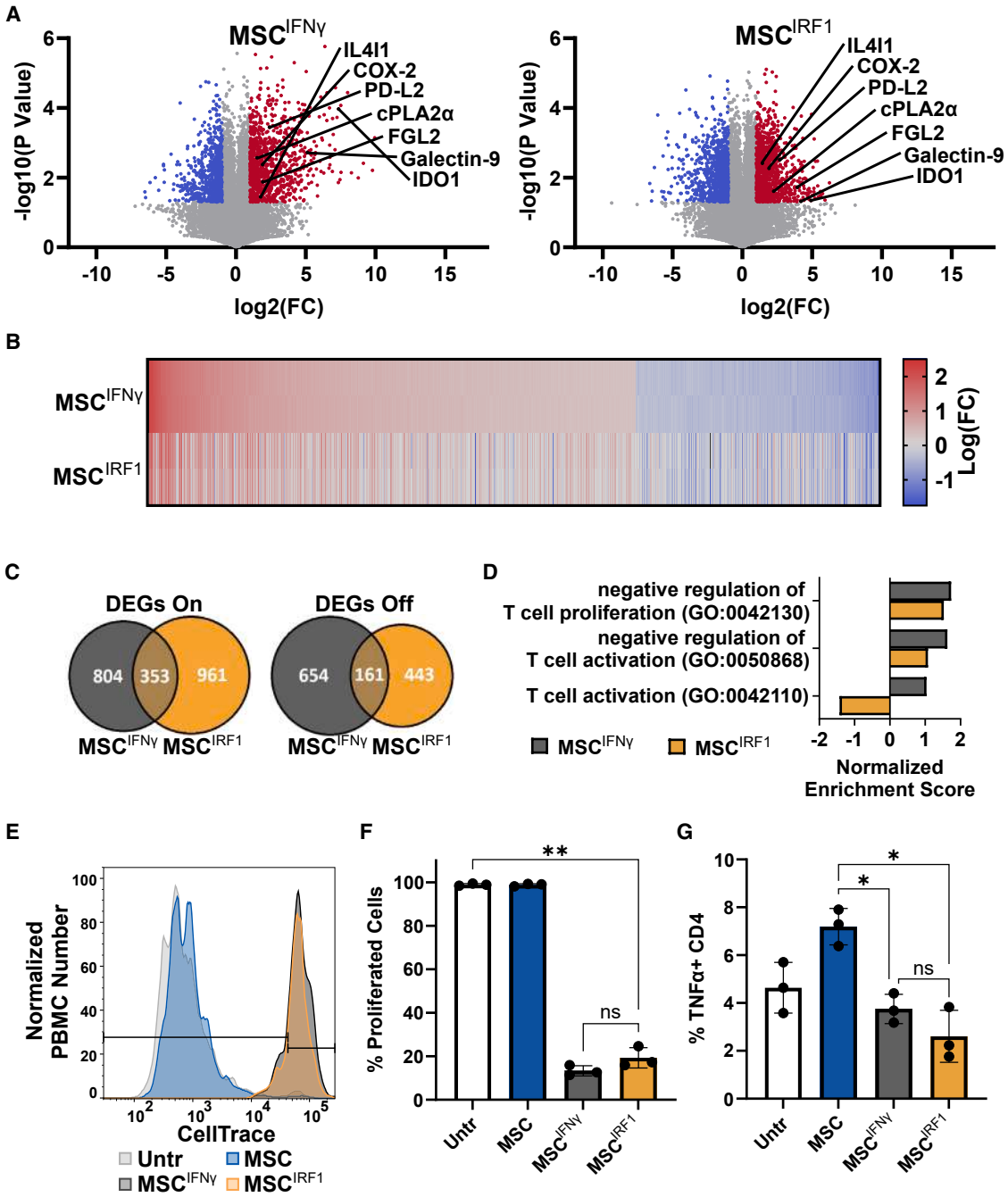

Figure 2. MSC^{IRF1} recapitulates signatures of MSC$^{IFN\text{-}\gamma}$ activation and T cell suppression

(A) Volcano plot from RNA-seq analyses for MSC$^{IFN\text{-}\gamma}$ (left) and MSC^{IRF1} (right). Red and blue regions denote down and up-regulated DEGs respectively (FC > 2; $p < 0.05$). (B) Expression heatmap for DEGs identified for MSC$^{IFN\text{-}\gamma}$. Genes were ordered from highest to lowest FC. Corresponding FCs for MSC^{IRF1} are provided. (C) Venn diagram of all DEGs identified for MSC$^{IFN\text{-}\gamma}$ and MSC^{IRF1}. (D) Normalized enrichment scores for GO terms associated with T cells suppression/activation. (E and F) Suppression of T cell activation in flow cytometry based, CellTrace Violet dilution assays. T cells in PBMC cultures were activated using anti-CD3 and anti-CD28 antibodies and cultured with MSC CM. (G) CD4 T cells were found to express less TNF-α on a per-cell basis with CM from MSC$^{IFN\text{-}\gamma}$ and MSC^{IRF1} compared with unstimulated MSCs 3 days after exposure to MSC CM. One way ANOVA. *$p < 0.05$, **$p < 0.01$. ns, not significant. Error bars represent the SD.

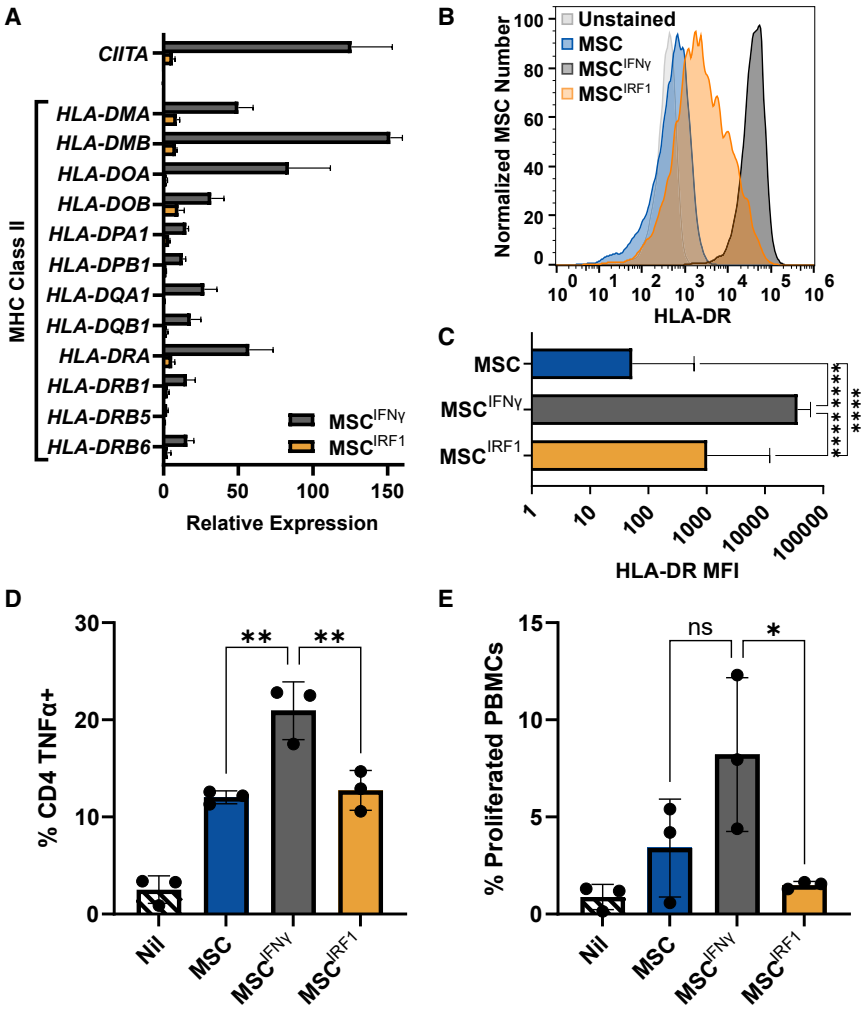

Figure 3. MSC^{IRF1} avoids MHC class II expression and subsequent CD4 T cell activation and proliferation present with MSC$^{IFN-\gamma}$

(A) Relative expression levels of CIITA and MHC class II genes for MSC$^{IFN-\gamma}$ and MSC^{IRF1} with respect to unprimed MSCs. (B and C) Flow cytometry analyses of HLA-DR surface expression. (D and E) Quantitation of TNF-α expression in CD4$^+$ T cells (D) and PBMC proliferation (E) upon direct co-culture with MSC$^{IFN-\gamma}$ than MSC^{IRF1} cells. Percent proliferation values were calculated using CellTrace Violet intensities. One-way ANOVA. *$p < 0.05$, **$p < 0.01$. ns, not significant. Error bars represent the SD.

bypass STAT1 phosphorylation and avoid upregulation of STAT1-responsive ISGs that are not activated by IRF1 alone, such as CIITA.

To further investigate functional consequences of the different activation modes in MSC^{IRF1} and MSC$^{IFN-\gamma}$ cells, high throughput imaging analyses were performed to quantitatively compare differences in primed cell morphologies (Figure 5). Prior reports have shown that IFN-γ can induce morphological changes that coincide with enhancement in immunosuppressive capacity.[52] We performed similar analyses using ER tracker dye to stain the MSC endoplasmic reticulum (ER), which extends throughout the cytoplasm, in addition to nuclear staining (Figures 5 and S6). Seven MSC morphological features were found to be significantly changed upon IFN-γ stimulation in this study. Six of these were replicated from previously documented morphological changes in the literature, and one of these was not previously studied. Significantly altered features included increases in ER compactness, convex area, perimeter, major axis length, and max feret diameter and decreases in ER form factor and nuclear to ER area ratio. MSC^{IRF1} morphology remained statistically similar to basal MSCs.

IRF1 can potentiate primary human MSCs activation persistently

We next examined the usefulness of IRF1 overexpression to sustainably activate the immunosuppressive properties of primary AD-MSCs (Figures 6 and S7–S12). Here, IRF1 overexpression was again observed to induce IDO1 transcription (Figure S8A) and translation (Figure 6A) and boost MSC production of kynurenine (Figure 6B). RNA-seq showed that IRF1-modified AD-MSCs also maintained transcriptional profiles that are required by the International Society for Cellular Therapy to designate cells as MSCs (Figure S8B). Moreover, RAP1 (*TERF2IP*) transcription, which has been reported to be necessary to retain MSC paracrine bioactivity,[28,53] was also unaffected and remained positive with IRF1 overexpression (Figure S8C). Finally, flow cytometry analyses show IRF1-modified primary AD-MSCs retain high levels of viability (>97%) (Figures S9A and S9B), although, as with chronic IFN-γ exposure in this experiment, IRF1-mediated genetic priming seems to decrease the proliferation rates (Figure S9C).

CM from IRF1-primed AD-MSCs was also capable of suppressing T cell proliferation in CellTrace dilution assays (Figures 6C, 6D, and S10). This suppression was accompanied by reduced activation of CD8$^+$ and CD4$^+$ T cells, signified by a loss of expression of IFN-γ and TNF-α, respectively (Figures 6E and 6F). Importantly, the CM in these experiments were also notably prepared using 5-fold fewer cells compared with the hTERT-MSC media, indicating that primary cells are not only amenable to IRF1-medated priming, but higher potencies can be achieved.

A second sample of commercially sourced primary AD-MSCs notably exhibited lower activation with respect to IDO1 expression (Figure S11A). IRF1-mediated priming responses were also attenuated appreciably in primary MSCs that were frozen and banked over short timescales (<7 days) (Figure S11A), indicating IRF1 activation can

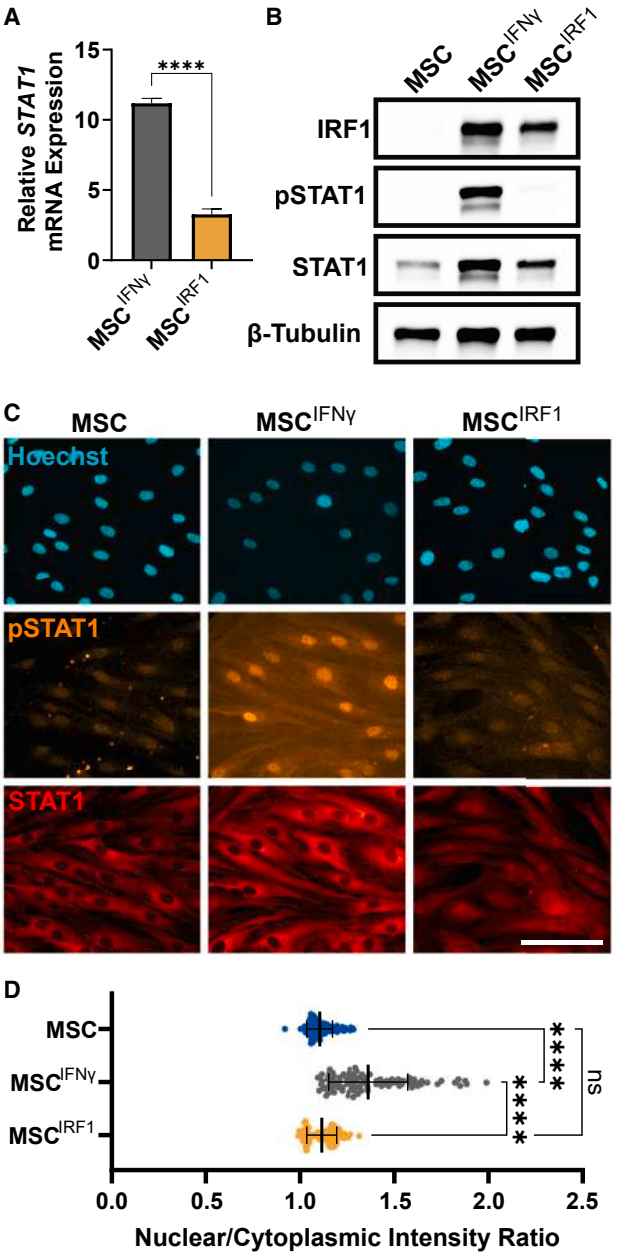

Figure 4. MSC^{IRF1} avoids STAT1 phosphorylation and subsequent signaling present in MSC$^{IFN\text{-}\gamma}$ in favor of nuclear localization of unphosphorylated STAT1

(A) Activation of STAT1 transcription by IFN-γ stimulation and IRF1 transgene overexpression. (B) Western blotting confirms STAT1 phosphorylation occurs in MSC$^{IFN\text{-}\gamma}$, but not MSC^{IRF1} or unprimed MSCs. (C) Immunocytochemical imaging of STAT1 and pSTAT1 localization. Images are contrasted equivalently. Scale bar, 100 μm. (D) Summary quantification of nuclear localization of pSTAT1. One-way ANOVA. Error bars represent the SD.$^{****}p < 0.0001$.

vary by MSC preparation and patient source. Nevertheless, IDO1 expression remained highly responsive to IFN-γ stimulation in these cells. We thus next tested whether IRF1-mediated genetic priming responses could be improved via brief stimulation with IFN-γ and/or budesonide, a glucocorticoid that is well known to potentiate MSC responses to IFN-γ[54] (Figure 7A). Our banked primary MSCs were transduced with IRF1 lentivirus, treated with IFN-γ and/or budesonide for 24 h, and then monitored by flow cytometry for IDO1 expression for 21 days. In contrast with biochemical priming alone (Figure 7B), all combinations of IFN-γ and/or budesonide with IRF1 overexpression were capable of yielding persistent IDO1 expression for at least 21 days (Figure 7C). Either IFN-γ or budesonide was found to increase the rates of IDO1 expression at early time points, indicating the potentiation of IRF1 transcriptional activity. We notably also demonstrated persistent, 21-day activation, can be achieved using iPSC-derived MSCs (Figures S11B and S11C).

Finally, while all treatments that included IFN-γ were found to upregulate the expression of HLA-DR, this was not the case with budesonide alone (Figure S12). Instead, the combination of IRF1 priming with budesonide was able to maintain the low levels of HLA-DR expression observed with basal, unprimed MSCs.

DISCUSSION

MSCs remain an attractive tool for cell therapy due to their unique abilities to secrete arrays of pleotropic immunomodulatory and restorative biomolecules. MSCs, however, require some form of biochemical or biophysical priming to activate the production of these molecules since they are not expressed appreciably without stimulation. Priming via pro-inflammatory cytokines such as IFN-γ to mimic the reciprocal interactions of MSCs with activated immune cells have been shown to induce broad changes to the MSC transcriptome and secretomes, and improve MSC potency.[15,16,20] Nevertheless, as demonstrated here and by others, IFN-γ-induced potency enhancements are very short lived and only last a few days.

This work demonstrates that the constitutive overexpression of the stimulus-responsive TF IRF1 can persistently activate MSC expression of many IFN-γ-responsive anti-inflammatory genes, including key immunomodulatory genes like *IDO1* and *PTGS2* (COX-2), as well as other negative regulators of T cell activation. Consistent with this profile, IRF1 overexpression MSCs were capable of suppressing T cell proliferation and activation in both hTERT-modified and primary human MSCs, yielding near equivalent potency found with IFN-γ priming.

IRF1-mediated priming was also found to circumvent the expression of the transcriptional activator CIITA, which is upregulated by IFN-γ and drives the expression of MHC class II genes known to potentiate MSC immunogenicity and clearance. We attribute this distinction to the role STAT1 plays in activating CIITA transcription, and the usefulness of IRF1 overexpression to circumvent the phosphorylation of STAT1 in the JAK/STAT pathway. While the relative roles of STAT1 and IRF1 in the upregulation of CIITA are found to vary depending on cell type,[55] the substantial activation of CIITA and downstream MHC class II genes by IFN-γ suggests STAT1 dominates this activation in MSCs. The overexpression of IRF1 was not found to influence

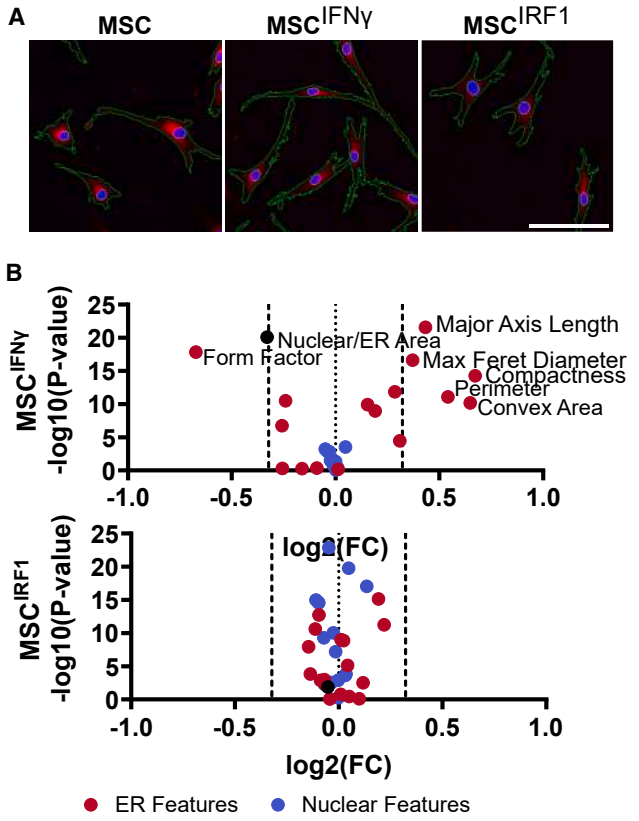

Figure 5. MSC^{IRF1} does not undergo morphological changes exhibited by MSC$^{IFN-\gamma}$

(A) Representative fluorescence images of ER (red) and nuclei (Hoechst/blue) in control MSCs, MSC^{IRF1}, and MSC$^{IFN-\gamma}$. The green lines depict cell edges determined via CellProfiler. Scale bar, 100 μm. (B) Volcano plots of measured changes in morphological features relative to unmodified naive MSC for MSC$^{IFN-\gamma}$ (top) and MSC^{IRF1} (bottom) show significant morphological adaptations occur in MSC$^{IFN-\gamma}$ that do not occur in MSC^{IRF1}. Dashed lines set to FC of 1.25.

STAT1 phosphorylation or nuclear localization appreciably via immunocytochemistry or western blotting analyses. Transient IRF1 expression has been reported to promote STAT1 activation in HEK cells.[56] However, our data do not support such effects in MSCs. Instead, the exogenously expressed IRF1 in the genetically primed MSC^{IRF1} cells seems to operate largely independent of the canonical STAT/JAK pathway, enabling selective activation of IRF1-responsive genes without upregulating pSTAT1.

We also demonstrated IRF1-mediated genetic priming can boost the immunomodulatory bioactivities of primary human MSCs. Here, the potency of CM from primary MSC^{IRF1} cells proved more potent compared with CM from hTERT modified MSC^{IRF1}, with approximately 5-fold fewer cells needed to achieve suppression effects equivalent to those with transient IFN-γ stimulation. Nevertheless, we also observed variability in IRF1-mediated priming responses across commercial MSC preparations, donor samples, and after freeze-thaw cycles. Responses were measured with respect to IDO1 expression, a key signature of MSC potency. Despite confirmation of efficient lentiviral transduction, IRF1-mediated induction of IDO1 seems to be times at times delayed in these cells. In contrast, the onset of IDO1 expression in primary MSCs was notably both rapidly and highly responsive to IFN-γ priming in all experiments, despite its subsequent decay.

Building on the hypothesis that the delayed MSC activation response stemmed from potential epigenetic effects that restrict IRF1 access to IRG loci in the absence of complete JAK/STAT signaling, we demonstrated efficient and persistent MSC activation can be achieved by combining IRF1-mediated genetic priming and brief stimulation with IFN-γ and/or pharmacological treatment using the corticosteroid budesonide. Both these transient treatments proved capable of accelerating MSC activation (IDO1 expression) appreciably. Moreover, constitutive IFR1 transgene expression was then able to take over and sustain IDO1 activation for at least 21 days, which is 4-fold longer than IFN-γ or IFN-γ plus budesonide. This persistent activation was also demonstrated using iPCS-derived MSCs, which are recognized for their potential off-the-shelf use in therapy and a resultant ability to circumvent issues surrounding MSC source and patient variability. Finally, while IFN-γ stimulation was naturally found to upregulate HLA-DR expression, the combination of budesonide and IRF1 overexpression minimized this activation, suggesting that this combination still circumvents activation of STAT1-responsive ISGs.

MSC treatments with budesonide and other glucocorticoids have been shown previously to enhance IFN-γ-induced IDO expression across multiple donors and in over-passaged cells.[54] In these studies, activation improvements were notably maximized with continuous exposure to budesonide. Our study shows that constitutive IRF1 expression can sustain this effect without additional pharmacological treatments. While the results with AD-MSCs and iPSC-MSCs are promising, additional studies are still needed to both optimize the usefulness of this approach within and across different MSC sources and validate the extent to which persistent genetic priming can boost MSCs efficacy *in vivo*. The attenuated proliferation due to IRF1 overexpression may be limiting and necessitate additional cell engineering. However, we expect this behavior to be much less problematic to approaches that incorporate MSCs within biomaterial hydrogels in order to contain and localize MSCs over the course of therapy.[57–59] These strategies naturally stand to benefit from persistently bolstered MSCs activation. Overall, we anticipate priming via manipulation of IRF1 and/or other stimulus-responsive TFs, individually and in combination, will ultimately facilitate tailored programming of the immunomodulatory and regenerative properties of the secretomes and associated modes of action of MSCs for specific cell therapy applications.

MATERIALS AND METHODS

MSC culture

Immortalized human adipose hTERT-MSCs, primary AD-MSCs, and iPSC-derived MSCs were obtained from the American Type Culture Collection (ATCC) (Manassas, VA, USA). hTERT-MSCs were

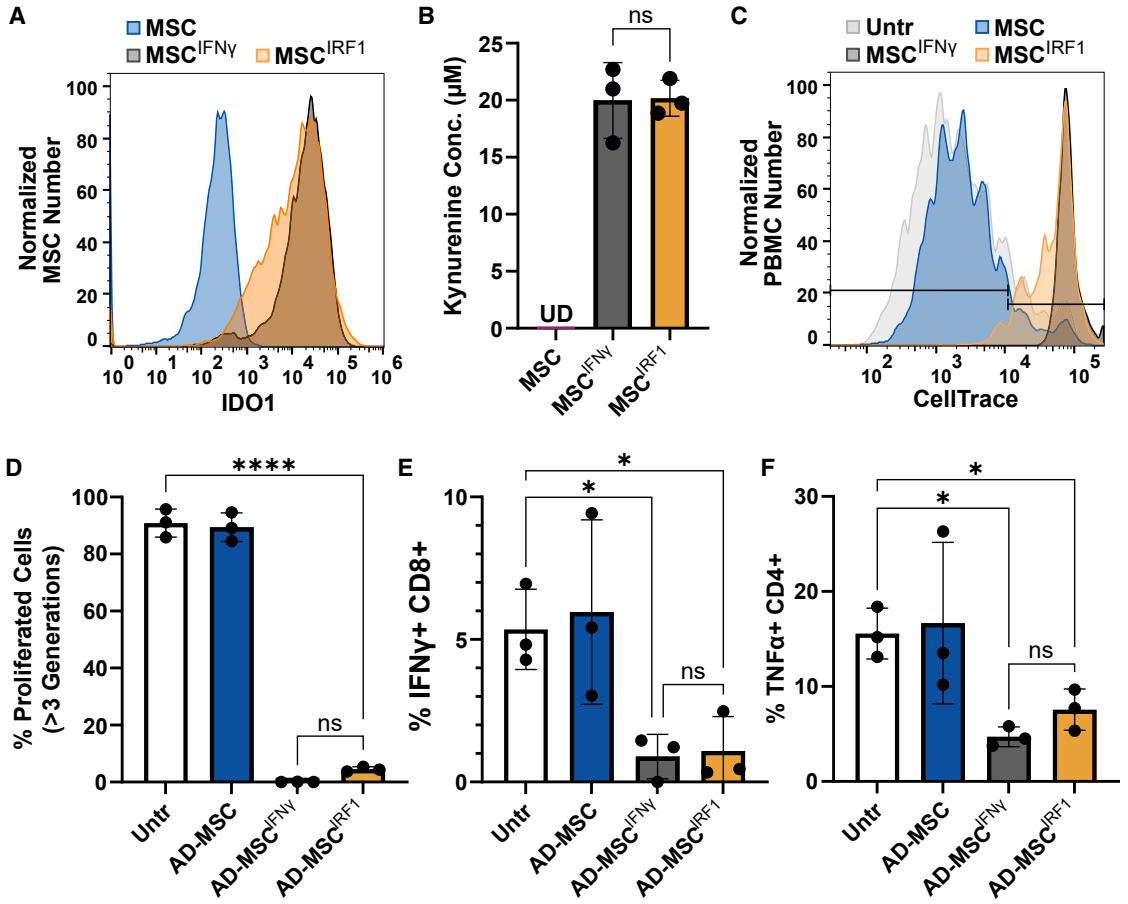

Figure 6. CM from primary MSC$^{IFN-\gamma}$ and MSC^{IRF1} abrogate T cell proliferation and activation

(A) IDO1 expression measured by flow cytometry shows IRF1 expression results in nearly as much IDO1 expression as IFN-γ stimulation. (B) Kynurenine production, an indicator of MSC activity, was high and indistinguishable between MSC$^{IFN-\gamma}$ and MSCIRF1. (C) MSC$^{IFN-\gamma}$ abrogated T cell proliferation slightly more than MSC^{IRF1}. Severe proliferation of more than 3 generations was abrogated by both MSC$^{IFN-\gamma}$ and MSC^{IRF1}. (D) Summary graph of (C). (E) MSC$^{IFN-\gamma}$ and MSC^{IRF1} were similar in their ability to minimize CD8 T cell activation via IFN-γ expression. (F) MSC$^{IFN-\gamma}$ and MSC^{IRF1} were similar in their ability to minimize CD4 T cell activation via TNF-α expression. One way ANOVA. *$p < 0.05$, ****$p < 0.0001$. ns, not significant. Error bars represent the SD.

maintained between passage 2 and 15 in DMEM (Gibco, Carlsbad, CA, USA) with 10% fetal bovine serum (FBS; Corning, Corning, NY, USA) and 1% antibiotic-antimycotic (Gibco, Carlsbad, CA, USA). For AD-MSCs, genetic priming effects were characterized in separate batches of MSCs from ATCC from two different lots. For iPSC-derived MSCs, one lot from ATCC was used. AD-MSCs and iPSC-derived MSCs were maintained between passages 2 and 8 in Mesenchymal Stem Cell Basal Medium for Adipose, Umbilical, and Bone Marrow-derived MSCs (PCS-500-030, ATCC) with Mesenchymal Stem Cell Growth Kit for Adipose and Umbilical-derived MSCs - Low Serum (PCS-500-040, ATCC) Passaging was done using 0.25% trypsin for 5 min at 37°C. Primary MSCs were thawed immediately from the manufacturer and used in downstream experiments unless otherwise specified. In freeze-thaw experiments, primary MSCs were frozen at passage 3 in FBS with 10% DMSO before being thawed. MSCs were treated with human recombinant IFN-γ (PeproTech, Cranbury, NJ, USA) at a concentration of 50 ng/mL for 24 h where indicated unless otherwise specified.

Lentiviral MSC engineering

The human IRF1 viral vector was synthesized by VectorBuilder (Chicago, IL, USA). HEK293T cells were obtained from ATCC and maintained in the same media as the hTERT-MSCs between passage 2 and 30. The HEK cells were plated at 7.7E4 cells/cm^2 the day before transfection. For each transfection, 4.878 μg IRF1 lentiviral plasmid, 1.463 μg pMD2.G, and 3.659 μg psPAX2 (Addgene, Watertown, MA, USA) were transfected using JetPRIME (Polyplus, Illkirch, France). Media was exchanged for media containing 4 mM sodium butyrate after 8 h. Virus-containing media was harvested at 24 and 48 h, filtered with a 0.45-μm filter to remove cellular debris and concentrated (100×) using Lenti-X concentrator (Takara, San Jose, CA, USA). The resulting particles were resuspended in

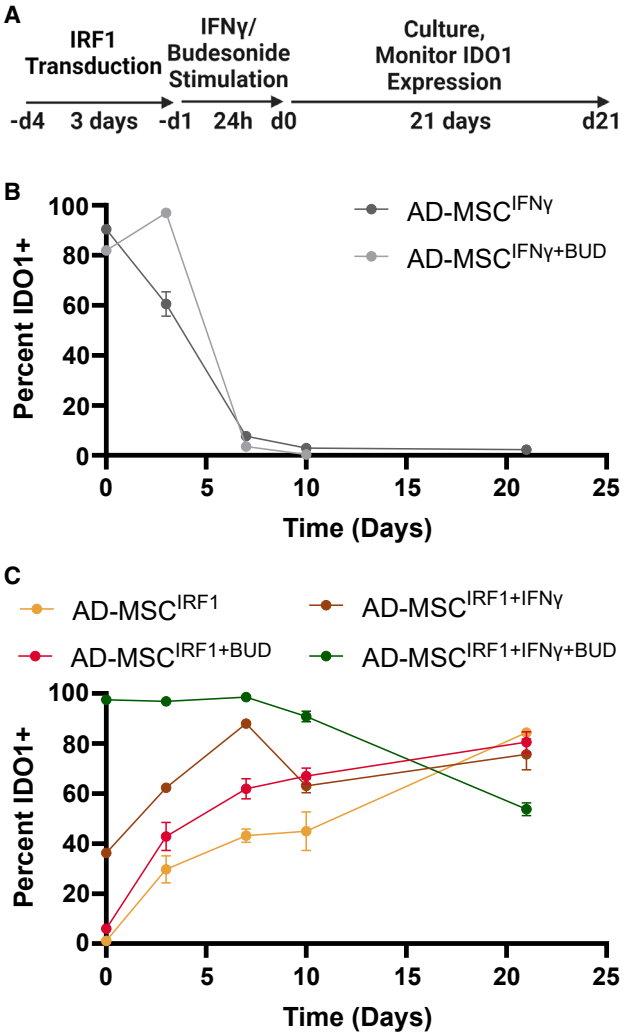

Figure 7. Persistence of IRF1 mediated MSC activation

(A) Experimental scheme for MSC transduction and transient treatment with IFN-γ and/or budesonide. (B) IDO1 expression responses in non-engineered MSCs that were primed biochemically with 50 ng/mL IFN-γ and/or with 1 μg/mL budesonide (BUD) for 24 h (C) The effect of IFN-γ and/or budesonide on the activation and persistence of IRF1-transduced MSCs. Percent positive IDO1 cells were determined by flow cytometry. Error bars represent the SD, $n = 3$.

DMEM with 10% FBS, 1% antibiotic-antimycotic and stored at −80°C.

The IRF1 lentivirus was reverse transduced into immortalized or primary MSCs in a six-well plate. MSCs between passages 2 and 5 were added onto the lentivirus and 10 mM polybrene was added to each well. Cells were then incubated for 72 h, their media were changed, and they were incubated for another 3–72 h before their GFP production was assessed by flow cytometry to determine transduction efficiency. An MOI of 1 was the minimum viral volume to obtain approximately 100% GFP positive cells. This viral volume (MOI = 1) was used in replicate reverse transduction process to make biological replicates of transgenic IRF1 MSCs that were used in downstream experiments. Transduction efficiencies were confirmed via fluorescence imaging.

RT-qPCR

Immortalized human adipose MSCs were plated in 6 well plates and rested for 24 h, after which, cells were lysed, and RNA was extracted using a RNeasy Mini Kit (Qiagen, Germantown, MD, USA). RNA was reverse transcribed to cDNA using an iScript cDNA Synthesis Kit (Bio-Rad, Hercules, CA, USA). qPCR was conducted using SsoAdvanced Universal SYBR Green Supermix (Bio-Rad) and the following primers (IDT, Newark, NJ, USA):

IRF1 F: 5′-CTCTCCCCGACTGGCACATC-3′

IRF1 R: 5′-CCGACTGCTCCAAGAGCTTCA-3′

IDO1 F: 5′-ACGGGACACTTTGCTAAAGGC-3′

IDO1 R: 5′-GGTTGCCTTTCCAGCCAGACA-3′

GAPDH F: 5′-CAATGACCCCTTCATTGACC-3′

GAPDH R: 5′-TTGATTTTGGAGGGATCTCG-3′

RNA-seq

RNA-seq experiments were performed in duplicate. RNA was extracted using an RNEasy Mini Kit and frozen at −20°C and sent to Azenta (Burlington, MA, USA) for whole RNA-seq. FASTQ files were processed using Galaxy to quantify read counts for each gene and condition. R and Python were used to convert Ensemble gene IDs to gene symbols. Python and the GSEAPY package were used to conduct GO enrichment analyses.

Western blotting

MSCs were lysed in RNA immunoprecipitation buffer. Total protein concentrations were quantified using a BCA assay. We loaded 25 μg protein for SDS-PAGE and transferred onto a PVDF membrane for western blot. Primary antibodies for STAT1 (66545-1, Proteintech, Rosemont, IL, USA) and pSTAT1 (MA5-15071, Thermo Fisher Scientific, Waltham, MA, USA) were used at a 1:5,000 and 1:1,000 dilutions, respectively, in 1× Tris-buffered saline with 1% casein (Bio-Rad). Secondary α-mouse horseradish peroxidase (HRP) (A6154, Sigma-Aldrich, St. Louis, MO, USA) or α-rabbit HRP (ab6721, Abcam, Cambridge, UK) were used at a 1:3,000 dilution in 1× Tris-buffered saline with 1% casein. Membranes were exposed after addition of ECL (170-5060, Bio-Rad). Tubulin was detected with hFAB Rhodamine Anti-Tubulin Primary Antibody (12004166, Bio-Rad) at 1:3,000 dilution.

Immunocytochemistry

MSCs were plated in six-well plates containing coverslips, cultured for 24 h, and fixed with 4% PFA in PBS for 20 min at 4°C–8°C. Cells were washed thoroughly with 0.2-μm filtered 5% BSA in PBS (blocking

solution), and permeabilized by incubation in 0.2% Triton X-100 in PBS at room temperature for 5 min. After washing and incubating with blocking solution for 1 h, cells were immuno-stained overnight at 4°C–8°C with rabbit anti-human IRF1 antibody (1:1,000, ab243895, Abcam) or rabbit anti-human pSTAT1 (1:400, MA5-15071, Thermo Fisher Scientific) and mouse anti-human STAT1 (1:800, 66545-1, Proteintech) diluted in blocking buffer. Secondary antibody staining was performed using Cy5 Goat anti-rabbit (1:500, A10523, Thermo Fisher Scientific), AF 594 donkey anti-rabbit (1:500, A21207, Invitrogen, Waltham, MA, USA), or AF 647 goat anti-mouse (1:500, A21235, LTC, Carlsbad, CA, USA). Secondary staining solutions also contained Hoechst nuclear stain (1:10,000, 33342, Thermo Fisher Scientific). Cells were visualized with a Nikon Eclipse Ti2 at 60× magnification. Background subtraction was done using ImageJ and was performed identically for each fluorophore.

Flow cytometry

Cells were trypsinized, fixed using BD Cytoperm/Cytofix (BD, Franklin Lakes, NJ, USA), permeabilized with BD Perm/Wash Buffer, and stained at room temperature for 1 h using a PE-labeled mouse anti-IDO1 antibody (12-9477-42, Thermo Fisher Scientific) or a BV786-labeled mouse anti-human HLA-DR antibody (564041, BD) according to the manufacturer's instructions. Excess antibody was removed via centrifugation and supernatant removal. Fluorescence levels were then quantified.

Kynurenine production

Kynurenine concentration was assessed by Ehrlich reaction. We combined 100 μL CM with 50 μL 30 wt% trichloroacetic acid in water in a round-bottom 96-well plate. A standard curve of purified L-kynurenine (Sigma-Aldrich) dissolved in R10 media was also included. This mixture was spun down at 2200RCF. We combined 100 μL supernatant with fresh 2 wt% dimethylaminobenzaldehyde (Sigma-Aldrich) in glacial acetic acid (Thermo Fisher Scientific). This mixture was immediately read at 490 nm on a plate reader.

Suppression bioactivity assays

MSC CM was prepared by culturing primary MSCs (2×10^5 cells) or hTERT-MSCs (1×10^6 cells) in R10 media for 48–72 h (RPMI Medium 1640 (Gibco, Waltham, MA, USA) with 10% heat-inactivated FBS, 1% penicillin-streptomycin (Gibco, Grand Island, NY), 1% GlutaMAX Supplement (Gibco, Grand Island, NY), 1% sodium pyruvate 100 mM (Gibco, Grand Island, NY), 1% HEPES 1 M (Gibco, Grand Island, NY), 1% MEM non-essential amino acids (Gibco, Grand Island, NY) for 48 and 72 h, respectively. CM was used directly without storage in subsequent assays. Human PBMCs were prepared from buffy coats obtained from Gulf Coast Regional Blood Center (Houston, TX, USA). Buffy coats were frozen and stored in liquid nitrogen before being thawed just before use. Viability was measured by AOPI (Nexcelom, Lawrence, MA, USA) and was required to be greater than 90% at thaw.

T cells were activated by incubating PBMCs with anti-CD3 (OKT3, Tonbo/Cytek, San Diego, CA, USA) and anti-CD28 (302934, Biolegend, San Diego, CA, USA) antibodies in PBS at 37°C for 3–5 h. For T cell proliferation analyses, PBMCs were stained with CellTrace Violet (Thermo Fisher Scientific) before activation.

TNF-α and IFN-γ expression levels were measured by treating PBMCs with GolgiPlug (Thermo Fisher Scientific) and GolgiStop (Thermo Fisher Scientific) to facilitate immunostaining analyses. PBMCs were fixed and permeabilized for 1 h at room temperature with Foxp3/TF Fix/Perm Concentrate and Diluent (Tonbo/Cytek), and then washed with Tonbo Flow Cytometry Perm Buffer (Tonbo/Cytek). Cells were then immuno-stained 1 h at room temperature with a panel of antibodies: anti-CD3 (563725, BD), anti-TNF-α (Biolegend 502938), anti-IFN-γ (Biolegend 506516), anti-perforin (Biolegend 506516), anti-T-bet (Biolegend 644812), and anti-Ki67 (BD 564071) for. Viable cells were identified using Ghost Dye Violet 510 (Tonbo/Cytek). Flow cytometry was performed using a BD LSRFortessa instrument. T cell proliferation and activation were quantified identically in MSC-PBMC co-culture experiments. In these experiments, MSCs were cultured for 3 days before PBMCs were placed in coculture for an additional 7 days. Media were changed every other day.

Immortalized human adipose MSCs were plated at 5.2E3 cells/cm^2 in 6 well plates. Cells were then stained with ER-Tracker Red (Thermo Fisher Scientific E34250) and Hoechst nuclear dye (Thermo Fisher Scientific 33342) according to manufacturer protocols. Cells were visualized using a Nikon Eclipse Ti2. A background subtraction method with a rolling ball radius and a contrast enhancement was done to better visualize cells in ImageJ. CellProfiler was used to identify cellular components. Nuclei and ER were identified by applying a size filter, separating clumped objects, and filling holes within objects. CellProlifer module MeasureObjectSizeShape was then used to measure morphological features of nuclei and ER. Subsequent data processing was done using MATLAB.

DATA AND CODE AVAILABILITY

All original data are available from the authors upon request.

SUPPLEMENTAL INFORMATION

Supplemental information can be found online at https://doi.org/10.1016/j.omtm.2024.101316.

ACKNOWLEDGMENTS

This work was supported by grants from the NSF (2041107) to M.R.D. and O.V. and the NIH (R21EB030772 and R35GM143532) to I.B.H. All graphics were created with BioRender.com.

AUTHOR CONTRIBUTIONS

M.A.B. and M.R.D conceived of the project. M.A.B., G.C.B., O.V., P.L.W., A.R.D., I.B.H., and M.R.D. designed experiments. M.A.B., G.C.B., D.A.B., L.D.S.S., T.N., A.R.D., S.C.L., and B.M. conducted experiments. M.A.B., G.C.B, L.D.S.S., and M.R.D. analyzed data. M.A.B. and M.R.D. wrote the manuscript. M.A.B., O.V., P.L.W., A.R.D., I.B.H., and M.R.D. edited the manuscript.

DECLARATION OF INTERESTS

The authors have submitted a pending provisional patent application related to this work.

REFERENCES

1. Zhuang, W.Z., Lin, Y.H., Su, L.J., Wu, M.S., Jeng, H.Y., Chang, H.C., Huang, Y.H., and Ling, T.Y. (2021). Mesenchymal stem/stromal cell-based therapy: mechanism, systemic safety and biodistribution for precision clinical applications. J. Biomed. Sci. *28*, 28.
2. Lotfy, A., AboQuella, N.M., and Wang, H. (2023). Mesenchymal stromal/stem cell (MSC)-derived exosomes in clinical trials. Stem Cell Res. Ther. *14*, 66.
3. Montero-Vilchez, T., Sierra-Sánchez, Á., Sanchez-Diaz, M., Quiñones-Vico, M.I., Sanabria-de-la-Torre, R., Martinez-Lopez, A., and Arias-Santiago, S. (2021). Mesenchymal Stromal Cell-Conditioned Medium for Skin Diseases: A Systematic Review. Front. Cell Dev. Biol. *9*, 654210.
4. Levy, O., Kuai, R., Siren, E.M.J., Bhere, D., Milton, Y., Nissar, N., De Biasio, M., Heinelt, M., Reeve, B., Abdi, R., et al. (2020). Shattering barriers toward clinically meaningful MSC therapies. Sci. Adv. *6*, eaba6884.
5. Gugliandolo, A., Bramanti, P., and Mazzon, E. (2020). Mesenchymal Stem Cells in Ms.pdf, pp. 1–35.
6. Eiro, N., Fraile, M., González-Jubete, A., González, L.O., and Vizoso, F.J. (2022). Mesenchymal (Stem) Stromal Cells Based as New Therapeutic Alternative in Inflammatory Bowel Disease: Basic Mechanisms, Experimental and Clinical Evidence, and Challenges. Int. J. Mol. Sci. *23*.
7. Guo, Y., Yu, Y., Hu, S., Chen, Y., and Shen, Z. (2020). The therapeutic potential of mesenchymal stem cells for cardiovascular diseases. Cell Death Dis. *11*, 349.
8. Yao, W., Shi, L., Zhang, Y., Dong, H., and Zhang, Y. (2022). Mesenchymal stem/stromal cell therapy for COVID-19 pneumonia: potential mechanisms, current clinical evidence, and future perspectives. Stem Cell Res. Ther. *13*, 124.
9. Pittenger, M.F., Discher, D.E., Péault, B.M., Phinney, D.G., Hare, J.M., and Caplan, A.I. (2019). Mesenchymal stem cell perspective: cell biology to clinical progress. npj Regen. Med. *4*, 22.
10. Han, Y., Yang, J., Fang, J., Zhou, Y., Candi, E., Wang, J., Hua, D., Shao, C., and Shi, Y. (2022). The secretion profile of mesenchymal stem cells and potential applications in treating human diseases. Signal Transduct. Targeted Ther. *7*, 92.
11. Li, P., Ou, Q., Shi, S., and Shao, C. (2023). Immunomodulatory properties of mesenchymal stem cells/dental stem cells and their therapeutic applications. Cell. Mol. Immunol. *20*, 558–569.
12. Ma, S., Xie, N., Li, W., Yuan, B., Shi, Y., and Wang, Y. (2014). Immunobiology of mesenchymal stem cells. Cell Death Differ. *21*, 216–225.
13. Wright, A., Arthaud-Day, M.L., and Weiss, M.L. (2021). Therapeutic Use of Mesenchymal Stromal Cells: The Need for Inclusive Characterization Guidelines to Accommodate All Tissue Sources and Species. Front. Cell Dev. Biol. *9*, 632717.
14. Giri, J., and Galipeau, J. (2020). Mesenchymal stromal cell therapeutic potency is dependent upon viability, route of delivery, and immune match. Blood Adv. *4*, 1987–1997.
15. Kim, D.S., Jang, I.K., Lee, M.W., Ko, Y.J., Lee, D.H., Lee, J.W., Sung, K.W., Koo, H.H., and Yoo, K.H. (2018). Enhanced Immunosuppressive Properties of Human Mesenchymal Stem Cells Primed by Interferon-γ. EBioMedicine *28*, 261–273.
16. Almeida-Porada, G., Atala, A.J., and Porada, C.D. (2020). Therapeutic Mesenchymal Stromal Cells for Immunotherapy and for Gene and Drug Delivery. Mol. Ther. Methods Clin. Dev. *16*, 204–224.
17. Diaz, M.F., Vaidya, A.B., Evans, S.M., Lee, H.J., Aertker, B.M., Alexander, A.J., Price, K.M., Ozuna, J.A., Liao, G.P., Aroom, K.R., et al. (2017). Biomechanical forces promote immune regulatory function of bone marrow mesenchymal stromal cells. Stem Cell. *35*, 1259–1272.
18. Xu, Z., Lin, L., Fan, Y., Huselstein, C., De Isla, N., He, X., Chen, Y., and Li, Y. (2022). Secretome of Mesenchymal Stem Cells from Consecutive Hypoxic Cultures Promotes Resolution of Lung Inflammation by Reprogramming Anti-Inflammatory Macrophages. Int. J. Mol. Sci. *23*, 4333.
19. Kurte, M., Vega-Letter, A.M., Luz-Crawford, P., Djouad, F., Noël, D., Khoury, M., and Carrión, F. (2020). Time-dependent LPS exposure commands MSC immunoplasticity through TLR4 activation leading to opposite therapeutic outcome in EAE. Stem Cell Res. Ther. *11*, 416.
20. Chen, Z., Yao, M.W., Shen, Z.L., Li, S.D., Xing, W., Guo, W., Li, Z., Wu, X.F., Ao, L.Q., Lu, W.Y., et al. (2023). Interferon-gamma and tumor necrosis factor-alpha synergistically enhance the immunosuppressive capacity of human umbilical-cordderived mesenchymal stem cells by increasing PD-L1 expression. World J. Stem Cell. *15*, 787–806.
21. Noronha, N.D.C., Mizukami, A., Caliári-Oliveira, C., Cominal, J.G., Rocha, J.L.M., Covas, D.T., Swiech, K., and Malmegrim, K.C.R. (2019). Correction to: Priming approaches to improve the efficacy of mesenchymal stromal cell-based therapies. Stem Cell Res. Ther. *10*, 1–21.
22. Wiese, D.M., Wood, C.A., Ford, B.N., and Braid, L.R. (2022). Cytokine Activation Reveals Tissue-Imprinted Gene Profiles of Mesenchymal Stromal Cells. Front. Immunol. *13*, 917790.
23. Vigo, T., Procaccini, C., Ferrara, G., Baranzini, S., Oksenberg, J.R., Matarese, G., Diaspro, A., Kerlero de Rosbo, N., and Uccelli, A. (2017). IFN-γ orchestrates mesenchymal stem cell plasticity through the signal transducer and activator of transcription 1 and 3 and mammalian target of rapamycin pathways. J. Allergy Clin. Immunol. *139*, 1667–1676.
24. Michalska, A., Blaszczyk, K., Wesoly, J., and Bluyssen, H.A.R. (2018). A positive feedback amplifier circuit that regulates interferon (IFN)-stimulated gene expression and controls type I and type II IFN responses. Front. Immunol. *9*, 1135.
25. Ivashkiv, L.B., and Donlin, L.T. (2014). Regulation of type i interferon responses. Nat. Rev. Immunol. *14*, 36–49.
26. Ivashkiv, L.B. (2018). IFNγ: signalling, epigenetics and roles in immunity, metabolism, disease and cancer immunotherapy. Nat. Rev. Immunol. *18*, 545–558.
27. Rosain, J., Neehus, A.L., Manry, J., Yang, R., Le Pen, J., Daher, W., Liu, Z., Chan, Y.H., Tahuil, N., Türel, Ö., et al. (2023). Human IRF1 governs macrophagic IFN-γ immunity to mycobacteria. Cell *186*, 621–645.e33.
28. Zhang, Y., Chiu, S., Liang, X., Gao, F., Zhang, Z., Liao, S., Liang, Y., Chai, Y.H., Low, D.J.H., Tse, H.F., et al. (2015). Rap1-mediated nuclear factor-kappaB (NF-κB) activity regulates the paracrine capacity of mesenchymal stem cells in heart repair following infarction. Cell Death Dis. *1*, 15007.
29. Schmalzl, A., Leupold, T., Kreiss, L., Waldner, M., Schürmann, S., Neurath, M.F., Becker, C., and Wirtz, S. (2022). Interferon regulatory factor 1 (IRF-1) promotes intestinal group 3 innate lymphoid responses during Citrobacter rodentium infection. Nat. Commun. *13*, 5730.
30. Campbell, B.M., Charych, E., Lee, A.W., and Möller, T. (2014). Kynurenines in CNS disease: Regulation by inflammatory cytokines. Front. Neurosci. *8*, 12–22.
31. Chinnadurai, R., Rajan, D., Qayed, M., Arafat, D., Garcia, M., Liu, Y., Kugathasan, S., Anderson, L.J., Gibson, G., and Galipeau, J. (2018). Potency Analysis of Mesenchymal Stromal Cells Using a Combinatorial Assay Matrix Approach. Cell Rep. *22*, 2504–2517.
32. Lim, J.Y., Kim, B.S., Ryu, D.B., Kim, T.W., Park, G., and Min, C.K. (2021). The therapeutic efficacy of mesenchymal stromal cells on experimental colitis was improved by the IFN-γ and poly(I:C) priming through promoting the expression of indoleamine 2,3-dioxygenase. Stem Cell Res. Ther. *12*, 37.
33. Ling, W., Zhang, J., Yuan, Z., Ren, G., Zhang, L., Chen, X., Rabson, A.B., Roberts, A.I., Wang, Y., and Shi, Y. (2014). Mesenchymal stem cells use IDO to regulate immunity in tumor microenvironment. Cancer Res. *74*, 1576–1587.
34. Zimmermann, J.A., Hettiaratchi, M.H., and McDevitt, T.C. (2017). Enhanced Immunosuppression of T Cells by Sustained Presentation of Bioactive Interferon-γ Within Three-Dimensional Mesenchymal Stem Cell Constructs. Stem Cells Transl. Med. *6*, 223–237.
35. Gonzalez, Y.I.R., Lynch, P.J., Thompson, E.E., Stultz, B.G., and Hursh, D.A. (2017). In Vitro Cytokine Licensing Induces Persistent Permissive Chromatin at the IDO1 Promoter. Cytotherapy *18*, 1114–1128.
36. Tse, W.T., Pendleton, J.D., Beyer, W.M., Egalka, M.C., and Guinan, E.C. (2003). Suppression of allogeneic T-cell proliferation by human marrow stromal cells: implications in transplantation. Transplantation *75*, 389–397.

37. Stagg, J., Pommey, S., Eliopoulos, N., and Galipeau, J. (2006). Interferon-γ-stimulated marrow stromal cells: A new type of nonhematopoietic antigen-presenting cell. Blood *107*, 2570–2577.

38. Lee, S.J., Qin, H., and Benveniste, E.N. (2008). The IFN-γ-induced transcriptional program of the CIITA gene is inhibited by statins. Eur. J. Immunol. *38*, 2325–2336.

39. Alagesan, S., Sanz-Nogués, C., Chen, X., Creane, M., Ritter, T., Ceredig, R., O'Brien, T., and Griffin, M.D. (2018). Anti-donor antibody induction following intramuscular injections of allogeneic mesenchymal stromal cells. Immunol. Cell Biol. *96*, 536–548.

40. Xie, X., Yang, X., Wu, J., Tang, S., Yang, L., Fei, X., and Wang, M. (2022). Exosome from indoleamine 2,3-dioxygenase-overexpressing bone marrow mesenchymal stem cells accelerates repair process of ischemia/reperfusion-induced acute kidney injury by regulating macrophages polarization. Stem Cell Res. Ther. *13*, 367.

41. Li, D., Han, Y., Zhuang, Y., Fu, J., Liu, H., Shi, Q., and Ju, X. (2015). Overexpression of COX-2 but not indoleamine 2,3-dioxygenase-1 enhances the immunosuppressive ability of human umbilical cord-derived mesenchymal stem cells. Int. J. Mol. Med. *35*, 1309–1316.

42. Haghighitalab, A., Martin, M.M., Amin, A., Minaee, S., Bidkhori, H.R., Doeppner, T.R., and Bahrami, A.R. (2021). Investigating the effects of IDO1, PTGS2, and TGF-β1 overexpression on immunomodulatory properties of hTERT-MSCs and their extracellular vesicles. Sci. Rep. *11*, 1–19.

43. Song, N., Scholtemeijer, M., and Shah, K. (2020). Mesenchymal Stem Cell Immunomodulation: Mechanisms and Therapeutic Potential. Trends Pharmacol. Sci. *41*, 653–664.

44. Stone, T.W., and Williams, R.O. (2023). Interactions of Ido and the Kynurenine Pathway with Cell Transduction Systems and Metabolism at the Inflammation – Cancer Interface. Cancers *15*, 2895.

45. Thumkeo, D., Punyawatthananukool, S., Prasongtanakij, S., Matsuura, R., Arima, K., Nie, H., Yamamoto, R., Aoyama, N., Hamaguchi, H., Sugahara, S., et al. (2022). Article PGE 2 -EP2/EP4 signaling elicits immunosuppression by driving the mregDC-Treg axis in inflammatory tumor microenvironment ll PGE 2 -EP2/EP4 signaling elicits immunosuppression by driving the mregDC-Treg axis in inflammatory tumor microenvironm. Cell Rep. *39*, 110914.

46. Sadik, A., Somarribas Patterson, L.F., Öztürk, S., Mohapatra, S.R., Panitz, V., Secker, P.F., Pfänder, P., Loth, S., Salem, H., Prentzell, M.T., et al. (2020). IL4I1 Is a Metabolic Immune Checkpoint that Activates the AHR and Promotes Tumor Progression. Cell *182*, 1252–1270.e34.

47. Zhao, Y., Yu, D., Wang, H., Jin, W., Li, X., Hu, Y., Qin, Y., Kong, D., Li, G., Ellen, A., and Wang, H. (2022). Galectin-9 Mediates the Therapeutic Effect of Mesenchymal Stem Cells on Experimental Endotoxemia. Front. Cell Dev. Biol. *10*, 700702–700717.

48. Kim, S.N., Lee, H.-J., Jeon, M.-S., Yi, T., and Song, S.U. (2015). Galectin-9 is Involved in Immunosuppression Mediated by Human Bone Marrow-derived Clonal Mesenchymal Stem Cells. Immune Netw. *15*, 241–251.

49. Hurrell, B.P., Helou, D.G., Howard, E., Painter, J.D., Shafiei-Jahani, P., Sharpe, A.H., and Akbari, O. (2022). PD-L2 controls peripherally induced regulatory T cells by maintaining metabolic activity and Foxp3 stability. Nat. Commun. *13*, 5118.

50. Zhao, Q., Hu, J., Kong, L., Jiang, S., Tian, X., Wang, J., Hashizume, R., Jia, Z., Fowlkes, N.W., Yan, J., et al. (2023). FGL2-targeting T cells exhibit antitumor effects on glioblastoma and recruit tumor- speci fi c brain-resident memory T cells. Nature communications *14*, 735. https://doi.org/10.1038/s41467-023-36430-2.

51. Schröder, B. (2016). The multifaceted roles of the invariant chain CD74 — More than just a chaperone. Biochim. Biophys. Acta *1863*, 1269–1281.

52. Klinker, M.W., Marklein, R.A., Lo, J.L., Wei, C., and Bauer, S.R. (2017). Morphological Features of IFN- γ – Stimulated Mesenchymal Stromal Cells Predict Overall Immunosuppressive Capacity. Proc. Natl. Acad. Sci. USA *114*, E2598–E2607. https://doi.org/10.1073/pnas.1617933114.

53. Ding, Y., Liang, X., Zhang, Y., Yi, L., Shum, H.C., Chen, Q., Chan, B.P., Fan, H., Liu, Z., Tergaonkar, V., et al. (2018). Rap1 deficiency-provoked paracrine dysfunction impairs immunosuppressive potency of mesenchymal stem cells in allograft rejection of heart transplantation. Cell Death Dis. *9*, 386.

54. Ankrum, J.A., Dastidar, R.G., Ong, J.F., Levy, O., and Karp, J.M. (2014). Performance-enhanced mesenchymal stem cells via intracellular delivery of steroids. Sci. Rep. *4*, 4645.

55. Reith, W., LeibundGut-Landmann, S., and Waldburger, J.M. (2005). Regulation of MHC class II gene expression by the class II transactivator. Nat. Rev. Immunol. *5*, 793–806.

56. Zenke, K., Muroi, M., and Tanamoto, K.I. (2018). IRF1 supports DNA binding of STAT1 by promoting its phosphorylation. Immunol. Cell Biol. *96*, 1095–1103.

57. Ghanta, R.K., Aghlara-Fotovat, S., Pugazenthi, A., Ryan, C.T., Singh, V.P., Mathison, M., Jarvis, M.I., Mukherjee, S., Hernandez, A., and Veiseh, O. (2020). Immune-modulatory alginate protects mesenchymal stem cells for sustained delivery of reparative factors to ischemic myocardium. Biomater. Sci. *8*, 5061–5070.

58. Shi, G., Zhou, Y., Liu, W., Chen, C., Wei, Y., Yan, X., Wu, L., Wang, W., Sun, L., and Zhang, T. (2023). Bone-derived MSCs encapsulated in alginate hydrogel prevent collagen-induced arthritis in mice through the activation of adenosine A2A/2B receptors in tolerogenic dendritic cells. Acta Pharm. Sin. B *13*, 2778–2794.

59. Huang, Y., Li, X., and Yang, L. (2022). Hydrogel Encapsulation: Taking the Therapy of Mesenchymal Stem Cells and Their Derived Secretome to the Next Level. Front. Bioeng. Biotechnol. *10*, 1–9.